Biochemical Engineering Journal 176 (2021) 108180

Contents lists available at ScienceDirect

Biochemical Engineering Journal

journal homepage: www.elsevier.com/locate/bej

Regular article

Characteristics of bio-$CaCO_3$ from microbial bio-mineralization with different bacteria species

Chunxiang Qian [a,b,c,d], Xinwei Ren [a,b,c,d,*], Yafeng Rui [a,b,c,d,*], Kai Wang [a,b,c,d]

[a] School of Materials Science and Engineering, Southeast University, Nanjing 211189, China
[b] Research Center for Green construction Materials & Carbon Utilization, Southeast University, Nanjing 211189, China
[c] Key Lab of Microbial Bio-mineralization Technology,China Construction Materials Industry, Nanjing 211189, China
[d] Jiangsu Key Laboratory for Construction Materials, Southeast University, Nanjing 211189, China

ARTICLE INFO

Keywords:
Bio-$CaCO_3$
Crystalline form
Morphology
Size
Decomposition temperature
Adhesion force

ABSTRACT

Nowadays, MICP (Microbially Induced Calcite Precipitation) technology has broad application prospects in civil engineering, such as sand consolidation, crack healing in cement-based materials, solid waste treatment, etc. Nevertheless, there were no systematic studies on the difference of bio-$CaCO_3$ produced by different microbial strains. In this study, XRD, TEM, SEM, STA and AFM were used to investigate the differences in crystalline form, morphology, size, decomposition temperature, and adhesion force of mineralized products. Those products were produced by *Photosynthetic bacteria, Bacillus mucilaginosus, Bacillus alcalophilus, Bacillus pasteurii* and chemical pathway. The results showed that all four microbial pathways were more productive than the chemical pathway. The calcite crystals formed by the chemical pathway presented an oblique hexagonal lattice structure, while calcite crystals formed by four microbes presented a spherical or irregular polyhedral structure under the action of organic substrate. The calcite crystals formed by *Bacillus pasteurii* were smallest in size and those formed by *Photosynthetic bacteria* were the largest, and their crystalline sizes were smaller than that of calcite produced by chemical pathway. The decomposition temperature and adhesion force of chemical $CaCO_3$ were lower than that of bio-$CaCO_3$, with the highest decomposition temperature (765.80 ℃) and the largest adhesion force (68.91 nN) of calcite induced by *Bacillus pasteurii*.

1. Introduction

The earliest use of MICP technology dates back to 1992, A Kantzas, G Ferris and LG Stehmeier et al. [1,2] applied MICP technology to geotechnical engineering. In 2001, Ramachandran [3] utilized MICP technology to repair cracks in cement-based materials. In 2004, CX Qian et al. [4] proposed the MICP technology for the first time in China. The principle of MICP technology [5] is to utilize the metabolism of mineralized microbes to conduct mineralization reaction and induce the deposition of $CaCO_3$ (calcium carbonate). So far, MICP technology is developing rapidly, and its applications in sand consolidation [6,7], heavy metal passivation [8,9], dust treatment [10], and crack healing in cement-based materials [11,12] has been widely concerned all over the world.

In terms of sand consolidation, urease-producing bacteria liquid and cementation liquid are poured into the sand, and the $CaCO_3$ crystal produced by MICP can fill and cement the space between sand particles, so that the sand is consolidated and the strength, permeability, compressibility and other engineering properties of the sand are improved.

C Li et al. [13] cemented aeolian sand soil through MICP technology, and verified the feasibility of MICP-treated aeolian sandy soil in the application of bio-crusts in desert engineering. Average unconfined compress strength of MICP-treated aeolian sandy soil was 0.66 MPa, and average inner friction angle was 36°. SC Zhu et al. [14] co-cultured PasteuriiandB and CereusCS1 and consolidation coal dust by the mixed bacterial inoculant, the mixed bacterial inoculant manifested a stronger consolidation effect. JM Liang et al. [15] studied the consolidation performance and consolidation mechanism of mature fine-grained tailings assisted by MICP technology. After consolidation treatment, the undrained shear strength of MFT was significantly improved, which means MICP could effectively accelerate the consolidation of MFT.

In terms of heavy metal passivation, due to the release of urease by microbes, urea is catalytically hydrolyzed to carbonate and ammonium

* Corresponding authors at: School of Materials Science and Engineering, Southeast University, Nanjing 211189, China.
E-mail addresses: cxqian1@163.com (C. Qian), rxwstcqwe@163.com (X. Ren), ruiyafeng@163.com (Y. Rui).

https://doi.org/10.1016/j.bej.2021.108180
Received 26 February 2021; Received in revised form 6 August 2021; Accepted 8 August 2021
Available online 11 August 2021
1369-703X/

salts. Ammonium salts alkalize the microenvironment, react with free heavy metal ions, and promote the combination of calcium and carbonate to form calcite precipitation [16], so that the mobility of heavy metals and pollution caused by heavy metals are reduced.

V Achal et al. [17] added *S. ginsengisoli CR5* into the medium containing 50 mM As(III), it remediated 96.3% of arsenic at 7 days. Y Zhao et al. [18] studied the ability to remove Cd of carbonate and biomineralized microbe GZ-22 based on biosorption and MICP technology, the result showed that Cd was converted to $CdCO_3$ by GZ-22 based on MICP technology, and the removal rate of Cd reached the highest of 60.72%, which was higher than that of biosorption. J He et al. [19] used MICP technology to study the effect of stabilizing Pb(II) and Cr(VI) in Urosoluble Staphylococcus epidermidis, the results showed that the removal rates of Pb(II) and Cr(VI) reached 86% and 76.8%, and the reaction can convert heavy metal ions in solution into carbonate compounds.

In terms of dust treatment, microbe induces the mineralization reaction to generate $CaCO_3$ with bonding property, which can bond the particles on the road and inhibit the rise of dust. Therefore, MICP technology can be applied in the field of dust treatment.

AH Wang et al. [20] developed microbial dust suppressant based on MICP technology. The consolidation layer formed on the dust surface when the microbial dust suppressant was sprayed on it, so that dust particles on construction site had good resistance to wind erosion, water erosion and anti-aging. P Chen et al. [21] studied the two kinds of fly ash produced in the process of mechanical grate furnace and circulating fluidized bed incineration, and explored the applicability of MICP technology in treating fly ash from municipal solid waste incineration with high alkalinity and heavy metal toxicity. The results showed that the unconfined compressive strength of fly ash treated by MICP reached 0.385 MPa and 0.709 MPa, respectively, and MICP can reduce the leaching toxicity of heavy metals. M Naeimi et al. [22] compared and analyzed the biological treatment dust suppressant and the traditional dust suppressant, the results showed that the biological treatment dust suppressant based on MICP technology needed to control 70% of sand was much lower than that of traditional dust suppressant. In addition, the biological treatment dust suppressant had the advantages of environmental compatibility and relatively harmless to vehicles.

In the term of crack healing in cement-based materials, mineralized microbes can fill and repair cracks by inducing mineralization reaction when they are added into cement-based materials.

SM Moshtaghioun et al. [23] used bacteria to repair concrete containing limestone powder and natural zeolite, calcite produce by bacteria increased compressive strength, tensile strength, ultrasonic pulse velocity and electrical resistivity of concrete; SG Choi et al. [24] repaired cracks in mortar samples by MICP technology, the results showed that the permeability of mortar samples treated with MICP technology was reduced, and cracks with width lower than 0.52 mm could be completely repaired; P Jongvivatsakul et al. [25] used MICP technology to repair cracked mortar samples by applying healing agent to the surface of samples and confirmed the feasibility of bacterial cells to repair cement mortar cracks, the results showed that the compressive strength of the samples treated by MICP technology was increased by 43% compared with that of the cracked samples, and the water tightness was significantly improved.

At present, MICP technology has been applied in a variety of different fields, and researchers have fully studied the application of MICP technology in related fields. However, there are differences in the types of mineralized bacteria and mineralization pathways by different scholars in the study of MICP technology. So far, there is no systematic study on the difference of bio-$CaCO_3$ (calcium carbonate produced by microbes) produced by different mineralized pathways. In this regard, we will study four kinds of bacteria, which are *Photosynthetic bacteria*, *Bacillus mucilaginosus*, *Bacillus alcalophilus* and *Bacillus pasteurii*.

Photosynthetic bacteria (strain A) are the earliest prokaryotes that appeared on the earth with a lot of protein, coenzyme Q, and completed B vitamins [26], it plays a vital role in the carbon cycle and material transformation in nature. The morphology of the bacteria is diverse, mainly spherical, rod-shaped, spiral, and oval.

Bacillus mucilaginosus (strain B) is a gram-negative bacillus and its cell wall is composed of lipopolysaccharides (LPS), porin, and peptidoglycan. LPS are generally composed of three parts, which are hydrophobic lipoid A, core oligosaccharides, and O antigens composed of the repetitive sugar units. The microbe is rod shape with a thick capsule and large spore. The colony on the special medium plate is round with colorless and transparent, and its bulge is greater than 45 degrees. After 5–6 days of incubation, a turbidity point appeared in the middle of the bacterial colony, and the edge is transparent. The surface is smooth, thick, elastic and can be pulled into filaments.

Bacillus alcalophilus (strain C), which exists in soil and has no harm to human, is a facultative aerobic gram-positive bacillus with a bar shape [27]. It has strong adaptation to a highly alkaline environment and can be directly added to highly alkaline cement-based materials.

Bacillus pasteurii (strain D) can produce urease under certain conditions. Urease has absolute specificity and can catalyze the hydrolysis of substrate to release ammonia and carbon dioxide [28]. Urease is the metalloenzyme with nickel ions, whose molecular weight is about 120,000−130,000. With the presence of water, it can break down urea into ammonia and carbon dioxide. The maximum hydrolysis rate of urease is 2.0–4.0 mmol urea per hour with 1 milligram of zymoprotein, which is 1014 times faster than the reaction without urease catalysis.

In this research, the X-Ray Diffraction (XRD), Transmission Electron Microscope (TEM), Field emission scanning electron microscope (SEM), Synchronous thermal analyzer analysis (STA), Atomic force microscope (AFM) were used to investigate the difference in crystalline form, morphology, size, decomposition temperature and adhesive force of mineralized products formed by *Photosynthetic bacteria*, *Bacillus mucilaginosus*, *Bacillus alcalophilus*, *Bacillus pasteurii* and chemical pathway. Through comparison and analysis, established the corresponding relationship between the microbial bio-mineralization pathways and the characteristics of mineralized products.

2. Raw materials and methods

2.1. Species and culture of microbes

2.1.1. Choose of microbes

Microbes in nature secrete enzymes continuously in and out of cells during metabolism and change the ambient medium by enzyme catalyzed reaction. Microbes produce carbonate in the presence of a metal cation slowly, the process is called microbial mineralization. According to the mineralized mechanism of secreted enzymes, microbial mineralization can be classified into microbial photosynthesis mineralization, microbial carbon dioxide capture mineralization and microbial nitrogen cycle mineralization [29]. Based on the mineralized mechanisms, researchers typically select microbes that are relatively easy to control, have relatively short mineralization process time and are suitable to survive and reproduce in soil and building materials. In this study, *Photosynthetic bacteria*, *Bacillus mucilaginosus*, *Bacillus alcalophilus* and *Bacillus pasteurii* were chosen.

2.1.2. Microbial culture

The composition of the culture medium is shown in Table 1. Microbes were inoculated into the culture medium and incubating at 30 °C on a constant temperature oscillation incubator at 170 rpm for 48 h.

In the course of incubating, the optical density of the cell solution OD_{600} was measured by optical densitometer every 4 h. In the paper, the growth of bacteria is indicated by OD_{600}. The OD_{600} value was used to draw the bacterial growth curve, and the cell growth rate (h^{-1}) was calculated by the slope of the curve. When the optical density of the cell solution stopped increasing, the flow cytometry was used to measure the cell concentration (cells/ml).

Table 1
Liquid medium composition of four bacterial strains.

Nutritional ingredient	Strain A	Strain B	Strain C	Strain D
Sucrose	10.0 g	10.0 g	–	–
$Na_2HPO_4.12\ H_2O$	2.5 g	2.5 g	–	–
$MgSO_4$	0.5 g	0.5 g	–	–
$CaCO_3$	1.0 g	1.0 g	–	–
KCl	0.15 g	0.15 g	–	–
$(NH_4)_2SO_4$	0.5 g	0.5 g	–	–
Yeast extract	0.3 g	0.3 g	–	–
Peptone	–	–	5.0 g	5.0 g
Beef extract	–	–	3.0 g	3.0 g
Carbamide	–	–	–	20.0 g
Deionized water	1000 ml	1000 ml	1000 ml	1000 ml

2.2. Experiment of mineralization

2.2.1. Experimental process

In this experiment, mineralized products were produced by 4 pathways, which are strain A, strain B, strain C, strain D. The experimental schemes of the control group (chemical pathway) and four mineralization pathways are shown in Table 2. Strain A and strain B capture carbon dioxide from the air for mineralization. For these bacteria, we provided the carbon source from the outside in the experiment; Strain C and strain D break down the substrate to produce carbon dioxide for mineralization. For these bacteria, we provided the corresponding substrate in the experiment. The temperature was kept at 20 ℃. The steps of the experiment are as follows:

(1) 100 ml corresponding substrate solution was prepared in 5 different beakers. Bacterial solution was filtered by ordinary qualitative filter paper to remove the precipitation and retain the bacteria. Then, 100 ml filtrate containing bacteria was placed into the above four beakers, the remaining one was added with 100 ml deionized water as the control group.
(2) simulated solution in the beaker was mixed evenly and put into the sealed mineralization device. The device was pumped to a vacuum state and filled with oxygen of 90% purity. For strain A, strain B, and chemical pathway, three of the mineralization devices with beakers were connected the conical bottles, containing 10 ml 0.5 mol/L Na_2CO_3 solution and being connect with spherical funnels containing excess diluted hydrochloric acid. The rubber tube and spherical funnel were switched on, dilute hydrochloric acid was dropped to control the total amount of CO_2 in the mineralization device (as shown in Fig. 1). The carbon source of other mineralization devices was all provided by substrate decomposition. After calculation and adjustment, the total amount of carbon source provided by 5 beakers was the same.
(3) After 24 h of continuous mineralization, the mineralization devices were opened and the sediment from the beaker was filtered. Then the sediment was rinsed three times by deionized water and alcohol respectively to remove impurities.
(4) A vacuum drying oven was used to dry the precipitate at 30 ℃ for 24 h, then the sample was put into sealed bags.

Table 2
Conditions for different pathways.

Serial number	$CaCl_2$/g	Organic Calcium source/g	Urea /g	Deionized water/ml	Bacterial solution/ml
Chemical	1.11	0	0	200	0
A	1.11	0	0	100	100(strain A)
B	1.11	0	0	100	100(strain B)
C	0	3.08	0	100	100(strain C)
D	1.11	0	0.60	100	100(strain D)

2.2.2. Method for determination of calcium ions

In this experiment, the content of calcium ions was determined by EDTA titration. The principle is: Ca^{2+} is formed a coordination compound with calcium indicator and titrated with EDTA. EDTA grabs calcium ions from the indicator, making the solution appear the color of free indicator when the quantification point is reached. The steps of the experiment are as follows:

(1) 50 ml of the liquid under test was transferred into a 250 ml conical flask, KOH solution was added into the liquid to adjust the pH to 12;
(2) 0.2 g calcium-carboxylic acid indicator was added into the liquid;
(3) The liquid was titrated by EDTA standard titration solution. The dosage of EDTA standard titration solution was recorded when the color of the liquid changes from burgundy to bright blue;
(4) The content of calcium ion was calculated quantitatively by equation.

2.3. Characterization of mineralized products

2.3.1. X-ray diffraction analysis

The D8 Discover automatic XRD instrument produced by the Germany Bruker-Axs company was used to analyze the mineralized products. The test parameters were set as Cu-K_α target radiation, the wavelength was 0.154056 nm, the X-ray tube power was 40 kV × 30 mA, the step width was 0.02°, the scanning rate was 0.15 s/step, and 2θ angles of continuous scanning of samples was from 10° to 90°.

The powder samples required for testing were ground in an agate mortar and then passed 200 target quasi-sieve. Selected sieve residue and dried it in a vacuum drying oven for 24 h before X-ray diffraction test.

2.3.2. Transmission electron microscopy analysis

Tecnai G2 T20 transmission electron microscope produced by Czech FEI Company was used to analyze the mineralized products.

The samples were ground in an agate mortar and sieved to obtain powder particles with particle size less than 1 μm to avoid fluorescence and X-ray absorption. After sieving, the powder particles were put into anhydrous ethanol and dispersed for 60 s by vibration with an ultrasonic cleaner. After that, the particles were deposited on a carbon-based copper network for transmission electron microscopy analysis.

2.3.3. Field emission scanning electron microscope analysis

Sirion 200 field emission scanning electron microscope produced by FEI in the Netherlands was used to analyze the mineralized products.

The samples were ground in an agate mortar. After the ground powder sample was pasted to the sample stage with conductive adhesive, it needed to be handled by high resolution turbomolecular pumped sputter coater.

2.3.4. Synchronous thermal analyzer analysis

STA449 F3 synchronous thermal analyzer produced by NETZSCH company in Germany was used to analyze the mineralized products.

N_2 was used as a protective gas in this experiment, and the temperature rose rate in the experiment was 10 ℃/min, and stopped when the temperature rose to 1050 ℃.

2.3.5. Atomic force microscope analysis

Veeco Dimension ICON atomic force microscope produced by Null was used to analyze the mineralized products.

The sample were prepared into a circular flake with a diameter of about 10 mm by tablet press. In this paper, the interaction force (adhesion force) between $CaCO_3$ particles and probe was measured.

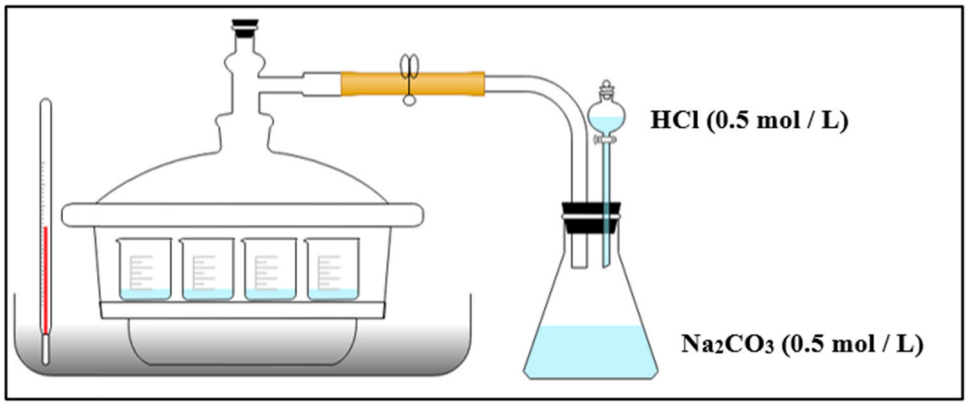

Fig. 1. Schematic diagram of mineralization device.

3. Results and discussion

3.1. Growth curves of bacteria

The growth of bacteria is indicated by the optical density OD_{600} of bacteria solution. The strain's growth curve is plotted with the culture time as the horizontal axis and OD_{600} as the vertical axis. The growth curves of the four strains are shown in Fig. 2. It illustrated that the growth of strains can be divided into lag phase, logarithmic phase and stationary phase. In the lag phase, the strain cell divided slowly and the bacteria concentration did not increase significantly. After the adjustment in the lag phase, the bacterial cells soon entered the logarithmic phase. In this phase, bacteria adapted to the new environment and had high metabolic activity; The number of bacteria increased exponentially until the growth rate reached the maximum. For strain A, the maximum rate of bacterial growth was 4.98×10^{-2} h^{-1}, while the rate was 7.51×10^{-2} h^{-1}, 5.75×10^{-2} h^{-1} and 4.69×10^{-2} h^{-1} when the microbe was strain B, strain C and strain D. Then, due to the consumption of nutrients and accumulation of harmful metabolites, the growth rate of cells began to slow down, and bacterial growth entered the stationary phase. At this time, the OD_{600} value of the bacteria solution was the highest. As a result of the number of newly proliferating bacteria and the dead bacteria gradually tended to be equal, the rate of bacterial growth tended to be zero. From Fig. 1, it can be observed that there was a difference of four microbes in growth. For strain A and strain B, the OD_{600} value of the bacteria solution was highest at 30 h, while the concentration of cells was about 9.6×10^8 cells/ml and 1.6×10^9 cells/ml at this time respectively. Besides, the OD_{600} value of the bacteria solution was highest at 28 h and 34 h when the microbe was strain C and strain D, while the concentration of cells was about 1.2×10^9 cells/ml and 1.1×10^9 cells/ml respectively. In this study, the cultured bacterial solution was used when OD_{600} reached highest.

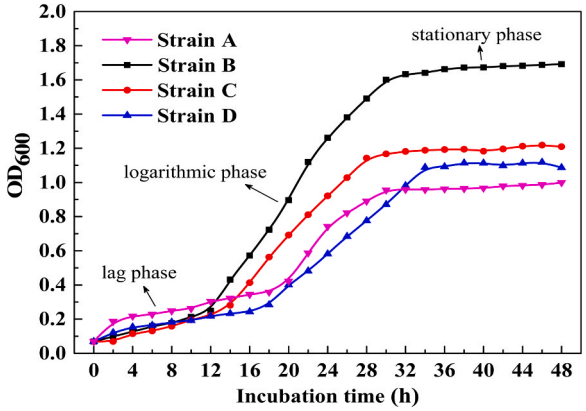

Fig. 2. Growth curves of four bacterial strains.

3.2. Formation of $CaCO_3$

In this study, we selected four species of bacteria with different mineralization mechanisms.

The mineralization mechanism of *Photosynthetic bacteria* (strain A) is that [30]: The bacteria break the balance of CO_3^{2-} and HCO_3^- ions in the aqueous solution by CO_2 dissolved in water, leading to the increase of pH. When Ca^{2+} are present in the aqueous solution, $CaCO_3$ is induced to produce. The mineralization mechanism is shown in Eqs. (1)–(4):

$$CO_2 + H_2O \rightarrow (CH_2O) + O_2 \quad (1)$$

$$2HCO_3^- \rightarrow CO_2 + CO_3^{2-} + H_2O \quad (2)$$

$$CO_3^{2-} + H_2O \rightarrow HCO_3^- + OH^- \quad (3)$$

$$Ca^{2+} + HCO_3^- + OH^- \rightarrow CaCO_3 + H_2O \quad (4)$$

The mineralization mechanism of *Bacillus mucilaginosus* (strain B) is that [31]: The bacteria secrete carbonic anhydrase with the effect of accelerating CO_2 hydration to produce HCO_3^-, and induce $CaCO_3$ deposition reaction. The mineralization mechanism is shown in Eqs. (5) and (6):

$$CO_2 + H_2O \rightarrow HCO_3^- + H^+ \quad (5)$$

$$Ca^{2+} + HCO_3^- + OH^- \rightarrow CaCO_3 + H_2O \quad (6)$$

The mineralization mechanism of *Bacillus alcalophilus* (strain C) is that [32]: The bacteria decompose organic calcium sources through aerobic respiration, producing $CaCO_3$ and CO_2. CO_2 reacts with Ca^{2+} in the environment to form $CaCO_3$. The mineralization mechanism is shown in Eqs. (7) and (8):

$$CaC_6H_{10}O_6 + 6O_2 \rightarrow CaCO_3 + 5CO_2 + 5H_2O \quad (7)$$

$$Ca^{2+} + OH^- + CO_2 \rightarrow CaCO_3 + H_2O \quad (8)$$

The mineralization mechanism of *Bacillus pasteurii* (strain D) is that [33]: The bacteria hydrolyze urea to produce CO_3^{2-}, which combines with Ca^{2+} to form $CaCO_3$. The mineralization mechanism is shown in Eqs. (9) and (10):

$$CO(NH_2)_2 + H_2O \rightarrow CO_2 + 2NH_3 \quad (9)$$

$$2NH_3 + CO_2 + H_2O \rightarrow 2NH_4^+ + CO_3^{2-} \quad (10)$$

During mineralization, the CO_3^{2-} concentration in the simulated solution increased continuously, then Ca^{2+} reacted with CO_3^{2} to produce $CaCO_3$, and caused the decrease of the Ca^{2+} concentration because CO_2 from air dissolved or substrate decomposed. The changes of Ca^{2+} concentration in the simulated solution under different microbial species

are shown in Fig. 3. From the figure, it can be seen that before 16 h, the Ca^{2+} concentration in the solution decreased at the fastest speed and gradually slowed down with time. After 30 h, the Ca^{2+} concentration basically tended to be stable, and $CaCO_3$ will no longer be deposited. Among them, the Ca^{2+} concentration decreased the most slowly in the chemical pathway. At the end of the reaction, the solution with the chemical pathway was highest in the Ca^{2+} concentration.

After 24 h of mineralization, the mineralization products were weighed by a precision balance (m_1). The mass of all Ca^{2+} in the simulated solution converted into $CaCO_3$ (m_2) was calculated. The mineralization rate of $CaCO_3$ in the simulated solution is m_1 /m_2.

Under different mineralization pathways, the mineralization rate of $CaCO_3$ in solution is shown in Fig. 4. It can be seen from the figure that the mineralization rate of bio-$CaCO_3$ was higher than that of chemical $CaCO_3$. This is because microbes act as the nucleation site in mineralization reaction, converging mineralization products and accelerating the deposition of mineralized products. The mineralization rate of strain D was the highest, while the mineralization rate was the lowest when the microbe was strain A. This result was consistent with the change rule of Ca^{2+} concentration in the solution in Fig. 3.

3.3. Crystalline form

The XRD pattern of precipitate generated by different pathways is shown in Fig. 5.

It can be seen from the XRD pattern that the positions of the main characteristic peaks were basically the same, which means the mineralized products are mainly calcite and a small part of vaterite. This is consistent with the current research status [34–36].

However, the strength of the main characteristic peaks was different. The peak strength of prominent characteristic peaks of calcite crystal induced by microbial pathways were lower than that of calcite crystal induced by the chemical pathway, indicating that the crystallization degree of products induced by microbial pathways was inferior.

The main crystal faces of calcite crystals formed by microbial pathways were (012), (104), (110), (113), (202) and (018). Among them, the calcite's growth orientation induced by strain C was most obvious on the crystal faces, while the growth orientation of the calcite induced by strain A was the weakest. The growth orientation of the calcite on the crystal face (104) was the strongest. On the crystal face (012), the growth orientation was the weakest, which is most evident in the calcite induced by strain A and strain B.

Lattice constants of the calcite crystals are shown in Table 3.

The electron diffraction spectra of calcite induced by chemical and microbial pathways are shown in Fig. 6. After calibrating to the diffraction pattern and calculation, it is found that the diffraction pattern calibration results obtained by chemical and microbial pathways are the closest to the lattice constant of PDF#05–0586, which is calcite.

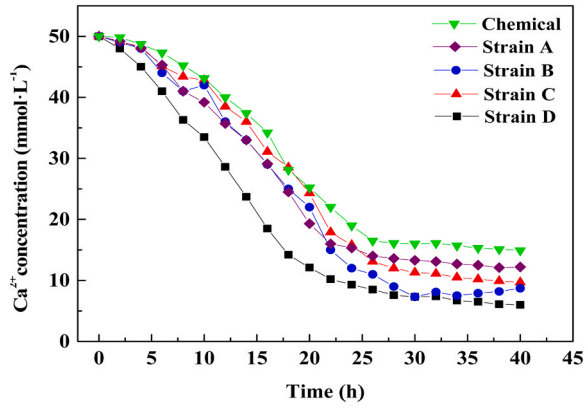

Fig. 3. The Ca^{2+} concentration of different pathways changes over time.

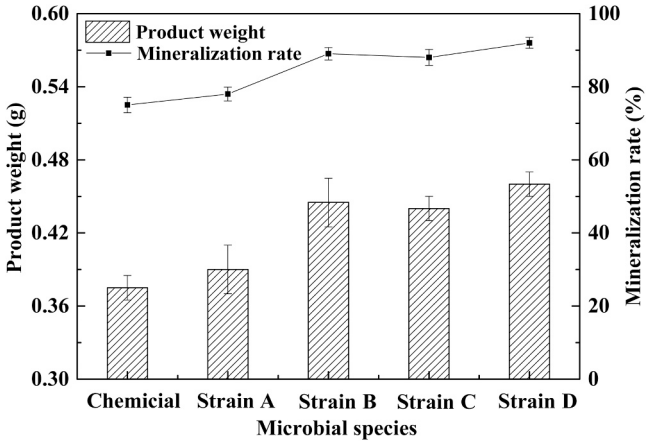

Fig. 4. Mineralization rate of $CaCO_3$ by different pathways.

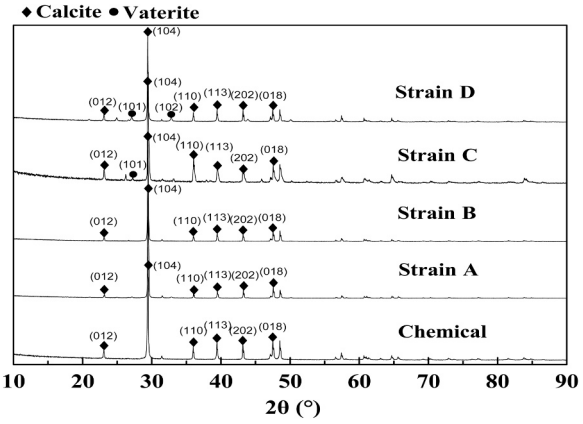

Fig. 5. XRD patterns of the sediments produced by different pathways.

Table 3
The lattice constants of calcite formed by different pathways.

Lattice parameters	Axis a	Axis b	Axis c
Chemical	4.985	4.985	17.038
Strain A	4.986	4.986	17.046
Strain B	4.987	4.987	17.064
Strain C	4.985	4.985	17.061
Strain D	4.986	4.986	17.068

This result is basically consistent with the results of calcium carbonate cell parameters refined by Jade 6.0 software.(Fig. 7).

3.4. Morphology

Fig. 8 showed the calcite's morphology induced by chemical and microbial pathways observed by SEM. The results showed that the morphology of precipitate obtained by different pathways was utterly different, which is consistent with existing research [36].

The crystals produced by the chemical pathway were developed in oblique hexagonal lattice structures. As shown in Fig. 8, the crystal particles were uniformly distributed with large size, showing flake or rhombic hexahedral single crystals, twin crystals, and their aggregates. The calcite induced by strain A contained polyhedrons with a small number of spherical particles, while the calcite induced by strain B was interlaced with polyhedral and spherical particles. The calcite appeared as irregularly shaped particles and spherical particles with uneven size when the microbe was strain C and strain D.

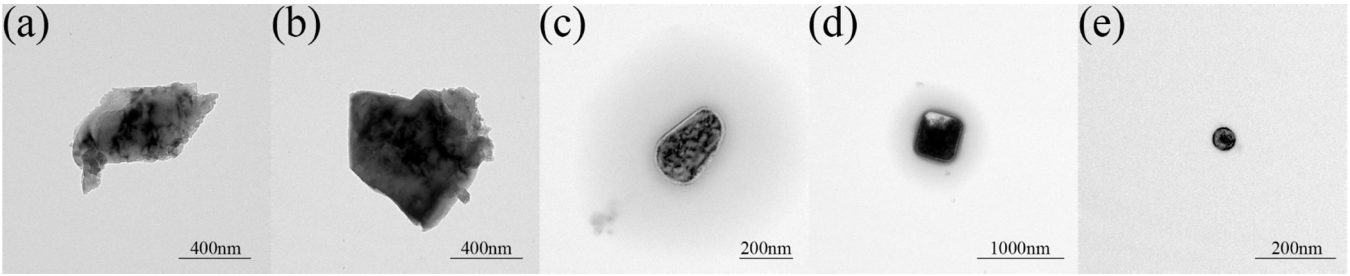

Fig. 6. Image plane of calcite produced by the different pathways under TEM. (a) chemical pathway; (b) strain A; (c) strain B; (d) strain C; (e) strain D.

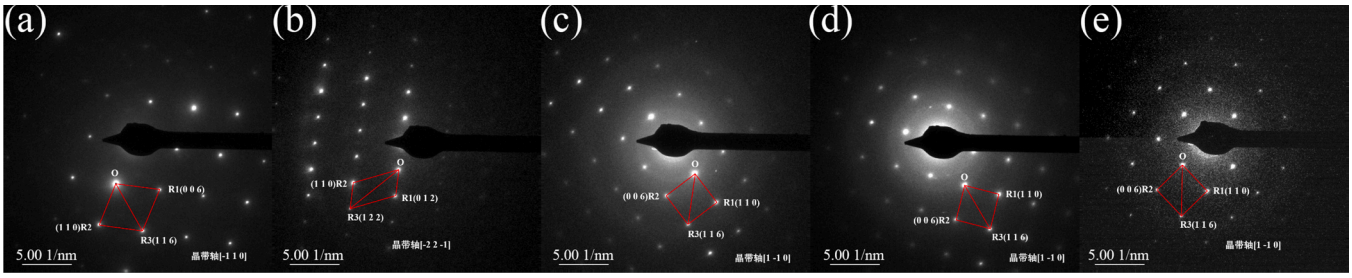

Fig. 7. Diffraction plane of calcite produced by the different pathways under TEM. (a) chemical pathway; (b) strain A; (c) strain B; (d) strain C; (e) strain D.

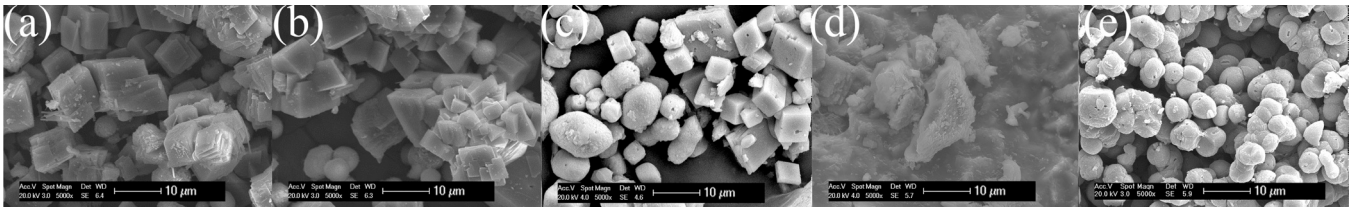

Fig. 8. Morphology of calcite produced by the different pathways. (a) chemical pathway; (b) strain A; (c) strain B; (d) strain D.

The morphology of crystal depends on the relative growth rate of crystal in different directions [37]. The growth rate is susceptible to the effects of foreign elements in the surrounding environment. Different parts of the lattice contacted with different external environments leading to different surface structures. The number of surface torsion zones, step zones and spiral dislocations, and the energy required for surface adhesion and ion binding are different, so that the growth rates are different [38].

During the formation of calcite crystals induced by different microbes, microbe produced different biological organic matter by the metabolism, including water-soluble organic matter (SM) and water-insoluble organic matter (IM). IM are mainly composed of hydrophobic proteins and polysaccharides, acting as skeletons. SM are commonly used as nucleation surfaces of bio-mineralization. The carboxyl residues in the organic matrix can chemically bond with Ca^{2+} [39], so calcite nucleation is precedent at the organic-inorganic interface. After the calcite nucleation, the growth of the crystal surface is prevented by adsorbing the organic substrates secreted by microbial selectively, the crystal surface which doesn't absorb the organic substrates continued to grow. The morphology of the crystal is changed by kinetic of growth. It is believed that there is a strong absorption between the organic substrate and the surface of $CaCO_3$, which limit the size of calcite crystal. Dispersed particles aggregate to form polycrystalline products, which grow in all directions along crystal axis C. Over time, the number of calcites that surrounded the cell and the organic matter secreted by the cell become more, causing fewer calcite crystals expand outward from the surface of the cell membrane, more calcite crystals grow outward along the direction of the crystals.

Researches [40] showed that SM and IM regulated the crystal morphology together. In addition, microbial secretions were the main factors affecting the morphology of calcite crystals, playing important roles in the form of mineralized products [41,42]. SM can be selectively adsorbed on specific crystal surfaces of calcite, change the relative growth rates of different crystal planes, and lead to changes in calcite crystals' habits, resulting in different morphology.

To better analyze the difference in the morphology of the calcite induced by the chemical and the microbial pathways, statistical methods were used to compare the morphology of the calcite. To perform the statistical method, three independent tests were conducted. Three detection zones were randomly observed under the scanning electron microscope for each sample, and the zones were shot at same depth of field and counted. The results showed that the morphology of calcite samples can be divided into three categories: spherical or ellipsoidal, polyhedron and irregular particles. The phase diagram and curve of the calcite morphology are shown in Figs. 9 and 10. It can be seen from the figure that the particles formed by the chemical pathway are mainly polyhedrons, and the morphology changes significantly after the participation of microbes. Among them, the calcite induced by strain D is mainly spherical and ellipsoidal.

3.5. Crystalline size

According to the X-ray diffraction theory, when the crystalline size of the sample is less than 100 nm, the diffraction peak width becomes significant as the crystalline size decreases, and the crystalline size of the sample can be calculated by Scherrer formula:

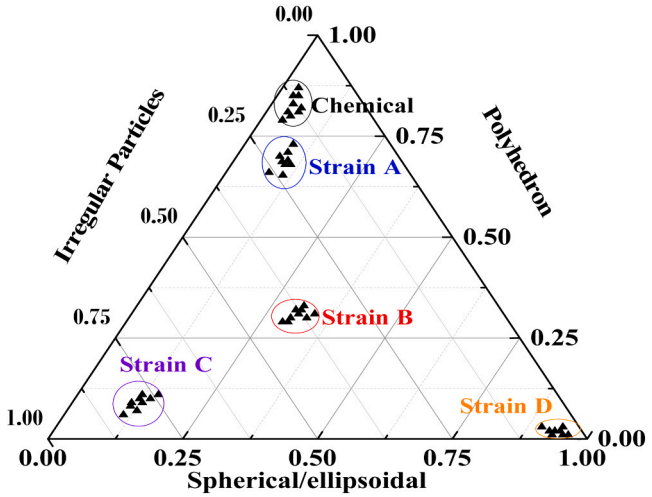

Fig. 9. Morphology and phase diagram of calcite produced by different pathways.

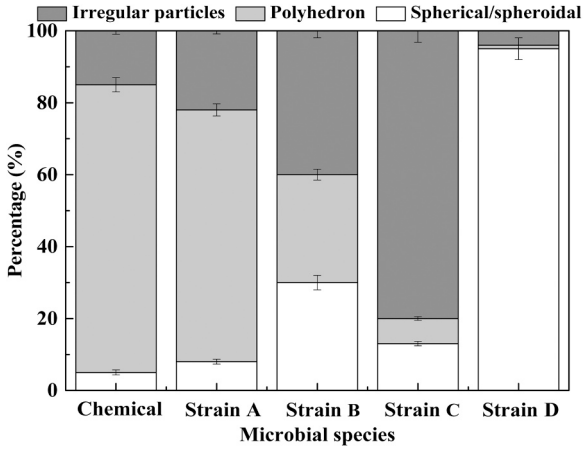

Fig. 10. Morphology curve of calcite produced by different pathways.

$$D = \frac{k\lambda}{\beta_{1/2}\cos\theta} \tag{11}$$

Where D is average crystalline size with unit of Å; k is coefficient with value of 0.89; λ is wavelength of the diffraction ray used in the experiment with value of 1.5406 Å; $\beta_{1/2}$ is half height and width of the selected diffraction peak with unit of rad; θ is diffraction Angle corresponding to the selected diffraction peak.

The Scherrer equation parameters of crystalline size are shown in Tables S1–S5. According to the results, it was shown that the crystalline size of calcite produced by the chemical pathway was 55.8 nm. The crystalline size of calcite induced by strain A was 46.5 nm, while the crystalline size of calcite induced by strain B was 38.3 nm. The crystalline size of calcite was 45.1 nm and 27.0 nm when the microbe was strain C and strain D. It can be seen that the crystalline size of calcite induced by the microbial pathways is smaller than that of calcite induced by the chemical pathway. Among them, the crystalline size of calcite induced by strain D was the smallest, while that of calcite induced by strain A was the largest.

To better analyze the difference in crystalline size between calcite produced by chemical and microbial pathways, statistical methods were used to analyze the results. The comparison of crystalline size of calcite produced by different pathways was shown in Fig. 11. It was seen that the rule of crystalline size obtained by statistical methods was consistent with that calculated by the Scherrer formula, while the statistical value

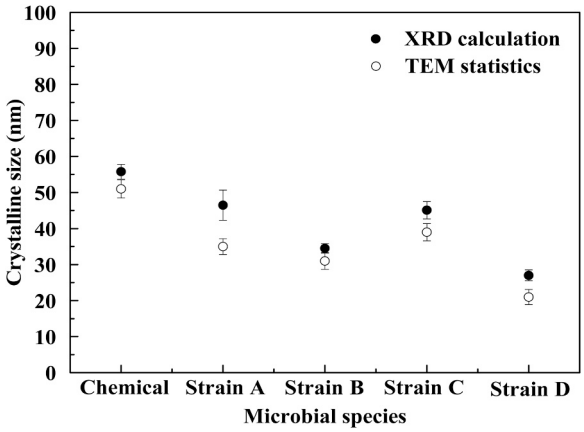

Fig. 11. Comparison of crystalline size of calcite produced by different pathways.

was slightly smaller than that calculated.

3.6. Particle size

The differences of calcite produced by different pathways in particle size is statistically analyzed, which is shown in Fig. 12. The figure showed that the particle size of calcite produced by the chemical pathway was smaller than that of calcite induced by microbial pathways, which was contrary to the rule of crystalline size. The particle size of calcite induced by strain C was the largest, while the particle size of calcite induced by strain A was the smallest.

After the nucleation of calcite crystal, the crystal surface's growth was prevented by organic substrate secreted by the microbes. Meanwhile, there is strong adsorption between the organic matrix and the surface of $CaCO_3$, and the adsorption limited the crystalline size of calcite [27]. Therefore, the crystalline size of calcite induced by microbial pathways was smaller than that of calcite induced by the chemical pathway. Besides, the dispersed particles form polycrystalline particle structures by the organic matter secreted by microbes, so the size of calcite particles produced by microbial pathways was larger than that by the chemical pathway.

3.7. Decomposition temperature

Fig. 13 showed the thermogravimetric curves of calcite produced by different mineralization pathways. It can be seen from Fig. 13 that the decomposition temperatures of calcite by different mineralization

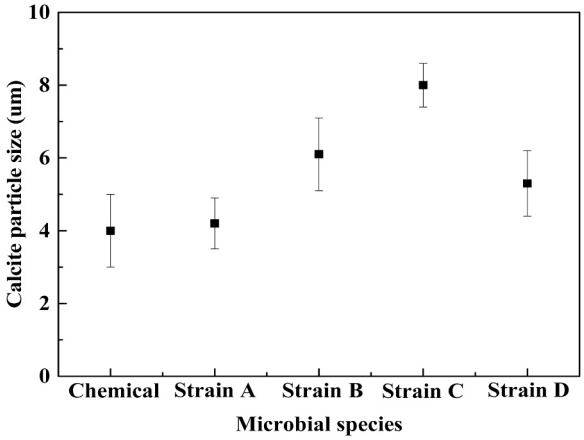

Fig. 12. Comparison of the sizes of calcite particles produced by different pathways.

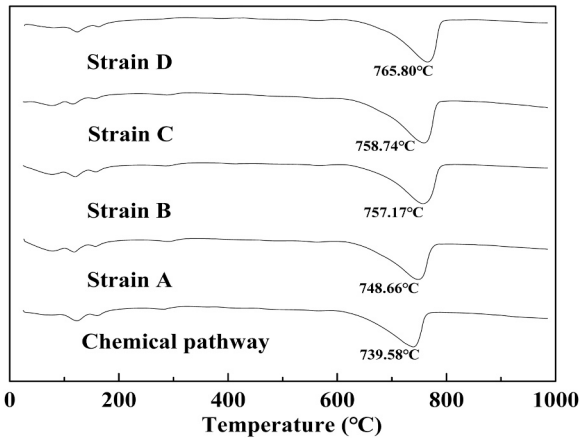

Fig. 13. Comparison of decomposition temperature of $CaCO_3$ in simulated solution of different microbial species.

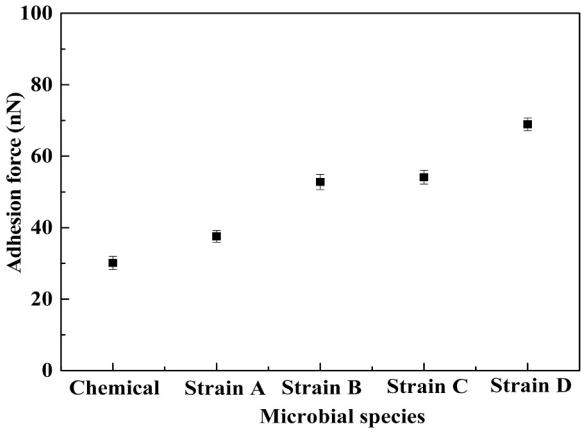

Fig. 14. Comparison of adhesion force of mineralized $CaCO_3$ produced by different pathways.

pathways were all in the range of 740–770 ℃, but that of calcite produced by chemical and microbial pathways were different. The decomposition temperature of calcite induced by strain A was 748.66 ℃, while the decomposition temperature was 757.17 ℃, 758.74 ℃ and 765.80 ℃ when the microbe was strain B, strain C and strain D, respectively. Besides, the decomposition temperature of calcite produced by the chemical pathway was 739.58 ℃, lower than that of calcite induced by microbial pathways, which is similar to existing research [43,44]. The maximum difference in decomposition temperature was 26.22 ℃. The calcite induced by different pathways had different properties, which were manifested as different decomposition temperatures on the macro level.

There are two possible reasons for the above phenomenon. One is the complex interaction between calcite and the organic substrate secreted by microbes, which cause the calcite induced by microbes different from that induced by the chemical pathway [45]. Because of the interactions, the calcite induced by microbes has cementing properties which is not found in the calcite produced by the chemical pathway. The special effect of microbial secreted organic substrate on calcite crystals is one of the reasons to cemented calcite together [27]. Therefore, when the calcite formed by microbial pathways decomposed, calcite needed to not only overcome its own chemical bond binding, but also overcome the special action binding. As a result, its decomposition temperature was higher than that of calcite formed by the chemical pathway. Different organic substrates secreted by different microbe led to different calcite decomposition temperatures.

Another reason is microbe's adsorption. When the peptidoglycan in microbial structure broke down at high temperatures, it generated carbon which added in calcite crystal structure, changing the shape of calcite crystal. This process raised the decomposition temperature of calcite. Hence, the decomposition temperature of calcite induced by microbe is higher than that of produced by the chemical pathway. The amount of carbon generated by different microbes during decomposition at high temperature is different, the way enter calcite crystal structure is different, and the changes of calcite are also different. Therefore, calcite induced by different microbes has different decomposition temperatures.

3.8. Adhesion force

Fig. 14 showed the comparison of the adhesion force of $CaCO_3$. It was found that the adhesion force of $CaCO_3$ induced by strain A was 37.56 nN. While, the adhesion force of $CaCO_3$ was 52.77 nN, 54.11 nN and 68.91 nN when the microbe was strain B, strain C and Strain D, respectively. Besides, the adhesion force of $CaCO_3$ induced by the chemical pathway was 30.12 nN.

Adhesion force of chemical $CaCO_3$ was less than that of bio-$CaCO_3$. Because microbes play the role of nucleation sites and accelerate the deposition of mineralized products [46]. Adhesion force of $CaCO_3$ induced by strain D was largest, while the adhesion force of $CaCO_3$ induced by strain A was minimum.

In this study, the effects of different mineralization pathways on the rate of mineralization were studied. As the nucleation site of mineralization reaction, microbes can converge mineralization products and accelerate the deposition of mineralized products. As a result of that, the mineralization rates of bio-$CaCO_3$ were higher compared to chemical $CaCO_3$, and the mineralization rates of four strains are different, which can be found from Fig. 4. Besides, the adhesion force of mineralized products is also affected by the action of bacterial nucleation sites. As Fig. 14 shown, adhesion force of chemical $CaCO_3$ was less than that of bio-$CaCO_3$. By comparing Fig. 4 with Fig. 14, it can be found that there is a certain relationship between the adhesion force and the mineralization rate of mineralized $CaCO_3$, the adhesion force of mineralized $CaCO_3$ increases with the increase of mineralization rate.

The properties of $CaCO_3$ induced by different mineralization pathways was also studied, which provided a suitable choice for other researchers to select bacteria using MICP technology in different application environment. Of the four bacteria we studied in this research, the adhesion force of mineralized $CaCO_3$ induced by *Bacillus pasteurii* is largest in four species of bacteria, it is suitable for self-repairing concrete, because the repair performance of concrete will improve when the adhesive force of repair products is higher.

4. Conclusion

In this study, the differences of the crystalline form, morphology, crystalline size, particle size, decomposition temperature, and adhesion force of $CaCO_3$ produced by different pathways were investigated. The main conclusions were as follows.

(1) The $CaCO_3$ produced by chemical and four microbial pathways was mainly calcite, but the main characteristic of calcite produced by microbial pathways had low peak strength, poor crystallization degree, and the C axis in lattice parameters enlarged.
(2) The calcite crystals produced by the chemical pathway were developed in an oblique hexagonal lattice structure, and the crystal particles size were uniformly distributed with large size, showing flake or rhombic hexahedral single crystals, twin crystals and their aggregates. The calcite induced by strain A contained polyhedrons with a small number of spherical particles, while the calcite induced by strain B was interlaced with polyhedral and spherical particles. The calcite appeared as irregularly shaped

particles and spherical particles with uneven size when the microbe was strain C and strain D.

(3) The crystalline size of calcite induced by microbial pathways was smaller than that of calcite produced by the chemical pathway, but the particle size of calcite was larger than that of calcite produced by the chemical pathway.

(4) The decomposition temperature of calcite produced by microbial pathways was higher than that produced by the chemical pathway, and the maximum difference in decomposition temperature was 26.22 ℃.

(5) The adhesion force of calcite produced by microbial pathways measured by atomic force microscope was higher than that produced by the chemical pathway.

CRediT authorship contribution statement

Qian Chunxiang: She directed the experiments, Provided writing ideas. **Ren Xinwei**: He was responsible for the collation and translation of the full text. **Rui Yafeng**: He given great help for the collation and translation of the full text. **Wang Kai**: He conducted experiments on microbial mineralization, and analyzed the characteristics of Bio-$CaCO_3$ from Microbial Bio-mineralization.

Declaration of Competing Interest

The authors declare that they have no known competing financial interests or personal relationships that could have appeared to influence the work reported in this paper.

Acknowledgment

The research was financially supported by key projects of National Natural Science Foundation of China: 51738003.

Appendix A. Supporting information

Supplementary data associated with this article can be found in the online version at doi:10.1016/j.bej.2021.108180.

References

[1] A. Kantzas, G. Ferris, K.N. Jha, A novel method of sand consolidation through bacteriogenic mineral plugging, Proc of CIM Annual Technical ConferenceCalgary, Canada: Petroleum Society of Canada, 1992.
[2] F.G. Ferris, L.G. Stehmeier, A. Kantzas, F.M. Mourits, Bacteriogenic mineral plugging, J. Can. Pet. Technol. 36 (1997).
[3] S.K. Ramachandran, V. Ramakrishnan, S.S. Bang, Remediation of concrete using microorganisms, Acids Mater. J. 98 (2001) 3–9.
[4] C.X. Qian, R.X. Wang, J.Y. Wang, Method for preparing calcium carbonate by microbial deposition.
[5] X.Z. Yuan, W. Sun, H.S. CHen, Research and development of microbiological repair technology for cement based material crack, J. Chin. Ceram. Soc. 37 (2009) 160–170.
[6] L.Y. Yin, C.S. Tang, Y.H. Xie, L. Chao, N.J. Jiang, B. Shi, Factors affecting improvement in engineering properties of geomaterials by microbial-induced calcite precipitation, 2019.
[7] L.I. Jin-Da, Research progress on microbial reinforcement soil technology.
[8] D. Zheng, Q. Dai, Y. Zhao, Y. Deng, F. Dong, Research Progress of Biomineralization in the Treatment of Heavy Metal Contamination, Research of Environmental ences, 2018.
[9] Z. Chen, X. Pan, H. Chen, X. Guan, Z. Lin, Biomineralization of Pb(II) into Pb-hydroxyapatite induced by Bacillus cereus 12-2 isolated from Lead-Zinc mine tailings, J. Hazard. Mater. 301 (2016) 531–537.
[10] Q. Zhan, C. Qian, Mineralization and cementation of fugitive dust based on the utilization of carbon dioxide and its characterization, J. Wuhan. Univ. Technol. (Mater. ence) 33 (2018) 263–267.
[11] T. Zheng, Y. Su, C. Qian, H. Zhou, Low alkali sulpho-aluminate cement encapsulated microbial spores for self-healing cement-based materials, Biochem. Eng. J. 163 (2020), 107756.
[12] M. Luo, C.X. Qian, R.Y. Li, Factors affecting crack repairing capacity of bacteria-based self-healing concrete, Constr. Build. Mater. 87 (2015) 1–7.
[13] L.I. Chi, S. Liu, T. Zhou, Y. Gao, D. Yao, The strength and porosity properties of micp-treated aeolian sandy soil, Mechanics in Engineering, 2017.
[14] S. Zhu, X. Hu, Y. Zhao, Y. Fan, S. Wang, Coal dust consolidation using calcium carbonate precipitation induced by treatment with mixed cultures of urease-producing bacteria, Water, Air, Soil Pollut. 231 (2020) 442.
[15] Z.G. Jiaming Liang, Lijun Deng, Yang Liu, Mature fine tailings consolidation through microbial induced calcium carbonate precipitation, Can. J. Civ. Eng. 42 (2015).
[16] W. Mwandira, K. Nakashima, S. Kawasaki, M. Ito, T. Sato, T. Igarashi, M. Chirwa, K. Banda, I. Nyambe, S. Nakayama, Solidification of sand by Pb(II)-tolerant bacteria for capping mine waste to control metallic dust: Case of the abandoned Kabwe Mine, Zambia, Chemosphere 228 (2019) 17–25.
[17] V. Achal, X. Pan, Q. Fu, D. Zhang, Biomineralization based remediation of As(III) contaminated soil by Sporosarcina ginsengisoli, J. Hazard. Mater. 201 (2012) 178–184.
[18] Y. Zhao, J. Yao, Z. Yuan, T. Wang, Y. Zhang, F. Wang, Bioremediation of Cd by strain GZ-22 isolated from mine soil based on biosorption and microbially induced carbonate precipitation, Environmental Science and Pollution Research, 2017.
[19] J. He, X. Chen, Q. Zhang, V. Achal, More effective immobilization of divalent lead than hexavalent chromium through carbonate mineralization by Staphylococcus epidermidis HJ2 - ScienceDirect, International Biodeterioration & Biodegradation, 140, 67–71.
[20] A. Wang, L. Fan, Discussion on the preparation and application of microbial dust suppressants, Shanxi Architecture, 2015.
[21] P. Chen, H. Zheng, H. Xu, Y.X. Gao, M.L. Ma, Microbial induced solidification and stabilization of municipal solid waste incineration fly ash with high alkalinity and heavy metal toxicity, PLoS One 14 (2019), 0223900.
[22] M. Naeimi, J. Chu, Comparison of conventional and bio-treated methods as a dust suppressant, Environ. Sci. Pollut. Res. 24 (2017) 23341–23350.
[23] S.M. Moshtaghioun, Use of bacteria for repairing cracks and improving properties of concrete containing limestone powder and natural zeolite, Constr. Build. Mater. 242 (2020).
[24] S.G. Choi, K. Wang, Z. Wen, J. Chu, Mortar crack repair using microbial induced calcite precipitation method, Cem. Concr. Compos. 83 (2017) 209–221.
[25] P. Jongvivatsakul, K. Janprasit, P. Nuaklong, W. Pungrasmi, S. Likitlersuang, Investigation of the crack healing performance in mortar using microbially induced calcium carbonate precipitation (MICP) method, Constr. Build. Mater. 212 (2019) 737–744.
[26] M. Han, X.S. Chen, L. Zhang, Y.J. Wang, Photosynthetic Bacteria and Their Applied Situation, Journal of Shenyang Agricultural University, 2002.
[27] E.W. Boyer, M.B. Ingle, G.D. Mercer, Bacillus alcalophilus subsp. halodurans subsp. nov.: an Alkaline-Amylase-Producing, Alkalophilic Organism, Int. J. Syst. Bacteriol. 23 (1973) 238–242.
[28] L. Alagna, S.S. Hasnain, B. Piggott, D.J. Williams, The nickel ion environment in jack bean urease, Biochem. J. 220 (1984) 591–595.
[29] R.X. Wang, Microbial Regulation of Calcium Carbonate Formation and its Application in Defect Repair of Cement-based Materials, Southeast University, 2009.
[30] S. Douglas, T.J. Beveridge, Mineral formation by bacteria in natural microbial communities, FEMS Microbiol. Ecol. 26 (1998) 79–88.
[31] B.K. Kanth, J. Lee, S.P. Pack, Carbonic anhydrase: Its biocatalytic mechanisms and functional properties for efficient CO_2 capture process development, Eng. Life Sci. 13 (2013) 422–431.
[32] V. Wiktor, H.M. Jonkers, Bacteria-based concrete: from concept to market, Smart Mater. Struct. 25 (2016), 084006.
[33] Subscribed Content Calcium Carbonate Precipitation by Ureolytic Subsurface Bacteria, Geomicrobiology Journal, 2000.
[34] E.V. Johnstone, S. Hofmann, A. Cherkouk, M. Schmidt, Study of the interaction of Eu3+ with microbiologically induced calcium carbonate precipitates using TRLFS, Environ. Sci. Technol. 50 (2016) 12411–12420.
[35] Y. Kim, Y. Roh, Microbially induced carbonate precipitation using microorganisms enriched from calcareous materials in marine environments and their metabolites, Minerals 9 (2019) 722.
[36] K.N. Jo, HuhMin, RohYul, 김유미, 서현희, 정다예, 신승원, carbonate biomineralization using speleothems and sediments from Baekasan Acheon Cave (Limestone Cave) in Hwasun-gun, Jeollanam-do, South Korea, Korean J. Mineral. Petrol. 31 (2018) 113–121.
[37] Z. Arifin, N.F. Apriliani, M. Zainuri, D. Darminto, Characterization of Precipitated $CaCO_3$ Synthesized from Dolomite, Materials Science & Engineering Conference Series (2017).
[38] F.Z. Cui, Biomineralization, Tsinghua University Press, 2012.
[39] H. Rong, Preparation and Cementation Mechanism of Microorganism Cement, Southeast University, 2014.
[40] J.M. Ouyang, Matrix Regulation and Biomimetic Application of Biomineralization, Chemical Industry Press, 2006.
[41] P. Li, W. Qu, Remediation of ancient masonry buildings by bacterially induced biomineralization, Building Structure, 2010.
[42] X. Tian, Y. Zhang, J. Zhang, Z. Ye, J. Lian, T. Duan, R. He, W. Zhu, Mineralization mechanism of mineralization bacteria on strontium crystallization of simulated radionuclides, Cryst. Res. Technol. 55 (2020), 1900133.
[43] H.H. Yi, C.X. Qian, Synthesis and characterization of calcium carbonate nanoparticles via bacterial mineralization in steel slag comprising cementitious materials, Sci. Adv. Mater. 12 (2020) 760–768.
[44] Z.Z. Han, D.X. Zhuang, H.X. Yan, H. Zhao, B. Sun, D. Li, Y.W. Sun, W.Y. Hu, Q. Z. Xuan, J.A. Chen, Y. Xiu, Thermogravimetric and kinetic analysis of thermal

decomposition characteristics of microbial calcites induced by cyanobacteria Synechocystis sp. PCC6803, J. Therm. Anal. Calorim. 127 (2017) 1371–1379.

[45] T. Zeng, K.T. Kim, C.J. Werth, L.E. Katz, K.K. Mohanty, Surfactant adsorption on shale samples: experiments and an additive model, Energy & Fuels, XXXX, 2020.

[46] H.H. Yi, Q.W. Zhan, C.X. Qian, Microbial-induced synthesis of mineralization products based on the capture of carbon dioxide: characteristics, reaction kinetics, interfacial adhesion properties, and mechanism of action, J. Chin. Chem. Soc. 66 (2019) 1589–1596.